Supporting Information

Effect of Zeolite Topology and Reactor Configuration on the Direct Conversion of CO_2 to Light Olefins and Aromatics

Authors: Adrian Ramirez[1], Abhishek Dutta Chowdhury[1], Abhay Dokania[1], Pieter Cnudde[2], Mustafa Caglayan[1], Irina Yarulina[1], Edy Abou-Hamad[3], Lieven Gevers[1], Samy Ould-Chikh[1], Kristof De Wispelaere[2] , Veronique van Speybroeck[2*] and Jorge Gascon[1*]

[1]King Abdullah University of Science and Technology, KAUST Catalysis Center (KCC), Advanced Catalytic Materials, Thuwal 23955, Saudi Arabia.

[2]Center for Molecular Modeling, Ghent University, Technologiepark 46, B-9052 Zwijnaarde, Belgium

[3]King Abdullah University of Science and Technology, Imaging and Characterization Core Labs, Thuwal 23955, Saudi Arabia.

Correspondence to: jorge.gascon@kaust.edu.sa

INDEX:

Figure S10. 1D ^{1}H-^{13}C cross-polarization MAS solid-state NMR spectra of zeolite trapped products, i.e. ZSM-5 and MOR.

Figure S11. Thermo-gravimetric analysis of the spent ZSM-5 and MOR zeolites.

Figure S12. 2D MAS ^{13}C-^{13}C solid-state NMR correlations identified zeolite ZSM-5 trapped molecular scaffolds.

Figure S13. ^{39}K solid-state NMR spectra at 21.1 T and 298 K of (a) post-reacted ZSM-5 and MOR samples.

Figure S14. Four adsorption states of 1-nonene.

Figure S15. Adsorption enthalpy at 350°C for 1-, 2-, 3-, 4-nonene and 2-nonyl carbenium ion in H-ZSM-5, H-MOR-1 and H-MOR-2.

Figure S16. Static geometries of adsorbed 1-nonene and 4-nonene π-complez in H-MFI, H-MOR-1 and right H-MOR-2.

Figure S17. Scatter plot of the mobility of 1-nonene and 4-nonene in the channel system of H-ZSM-5 during the 100 ps MD simulation at 350°C.

Figure S18. Scatter plot of the mobility of 1-nonene in H-MOR-1, 1-nonene in H-MOR-2, 4-nonene in H-MOR-1 and 4-nonene in H-MOR-2 in the channel system of MOR during the 100 ps MD simulation at 350°C.

Figure S19. Free energy profiles for the protonation of 1-nonene into a nonyl carbenium ion in H-ZSM-5 and H-MOR-1 at 350°C.

Figure S20. C_2–C_4 olefin STY ($mmol \cdot gcat^{-1} \cdot h^{-1}$) obtained in this work for the Fe_2O_3@KO_2/MOR catalyst compared to the best bifunctional catalysts available for CO_2 hydrogenation.

Figure S21. Aromatics STY ($mmol \cdot gcat^{-1} \cdot h^{-1}$) obtained in this work for the Fe_2O_3@KO_2/ZSM-5 catalyst compared to the best bifunctional catalysts available for CO_2 hydrogenation.

Table S1. Comparison of the state of the art bifunctional catalyst for the CO_2 hydrogenation towards olefin and/or aromatics.

Catalyst	GHSV (ml/h/gcat)	Conv (%)	Sel[a] CO (%)	Sel[a] C_1 (%)	Sel[a] C_2-C_4= (%)	Sel[a] Arom (%)	Ref [c]
In_2O_3-ZrO_2/SAPO-34	9000	35.5	85.0	0.6	11.5	N/A[b]	7
Na-Fe_3O_4/HZSM5	4000	34.0	15.0	6.9	3.4	36.5	8
In_2O_3-ZrO_2/SAPO-34	12000	21.5	90.0	0.8	9.0	N/A[b]	16
$ZnGa_2O_4$/SAPO-34	5400	13.0	49.0	N/A[b]	46.4	N/A[b]	17
In_2O_3-ZrO_2/SAPO-34	9000	35.5	85.0	0.6	11.5	N/A[b]	18
InZr/SAPO-34	9000	26.2	63.9	0.7	26.9	N/A[b]	19
ZnAlOx/ ZSM-5	4000	9.1	57.0	0.9	N/A[b]	35.6	20
Fused Fe/ZSM5	60	38.1	14.5	8.6	0.7	18.2	82
Cu-Zn-Cr/HY	3000	35.5	85.1	0.4	1.0	N/A[b]	83
Fe-ZnO/HY	3000	13.3	61.6	2.9	6.0	N/A[b]	84
Fe-K/KY	1900	21.3	26.5	11.2	23.2	N/A[b]	85
FeCuNa/H-MOR	3000	11.8	23.7	17.6	5.7	N/A[b]	86
Fe-Zn-Zr/HY	3000	17.2	53.2	1.4	4.7	N/A[b]	87
Fe/NaY	1900	20.8	29.4	10.2	22.6	N/A[b]	88
Fe-Ce/KY	1900	20.1	34.6	5.8	24.0	N/A[b]	89
Zn-ZrO_2/Zn-SAPO-34	3600	18.0	48.0	2.1	32.0	N/A[b]	90

[a] Total product selectivity.

[b] Data not available.

[c] Main text reference.

Table S2. Unit cell parameters of ZSM-5 and MOR.

	Zeolite	**a [Å]**	**b [Å]**	**c [Å]**	**α [°]**	**β [°]**	**γ [°]**
STATIC	ZSM-5	20.02	20.25	13.49	89.87	89.69	90.10
	MOR	18.29	20.29	14.97	89.96	90.10	90.14
MD	ZSM-5	20.22	20.35	13.58	90.00	89.91	90.06
	MOR	18.44	20.45	15.14	90.09	90.10	90.07

Table S3. Surface area (BET) and elemental composition of the ZMS-5 and MOR zeolites.

Zeolite	**Al (wt. %)**	**Na (wt. %)**	**Fe (wt. %)**	**K (wt. %)**	**Calculated SiO_2/Al_2O_3**	**Surface area (m^2/g)**
ZSM-5 (SiO_2/Al_2O_3=26)	2.39	0.02	0.26	0.01	35	366
ZSM-5 (SiO_2/Al_2O_3=52)	1.30	0.01	0.17	0.01	67	372
ZSM-5 (SiO_2/Al_2O_3=300)	0.22	0.01	0.03	0.00	406	368
ZSM-5 (SiO_2/Al_2O_3=600)	0.14	0.01	0.00	0.01	639	407
MOR	3.54	0.07	0.01	0.01	25	445

Table S4. Detailed catalytic performance of the Fe_2O_3@KO_2 material at 375 ºC, 30 bar, H_2/CO_2=3, and 10000 $mL \cdot g^{-1} \cdot h^{-1}$.

Conversion (%)	48.1
Sel CO (%)	15.9
Sel C1 (%)	15.2
Sel C2 (%)	1.6
Sel C2= (%)	8.1
Sel C3 (%)	1.3
Sel C3= (%)	10.9
Sel C4 (%)	1.3
Sel C4= (%)	9.2
Sel C5 (%)	0.8
Sel C5= (%)	7.6
Sel C6 (%)	0.1
Sel C6= (%)	6.4
Sel C7 (%)	0.5
Sel C7= (%)	6.1
Sel C8 (%)	0.3
Sel C8= (%)	3.5
Sel Benz (%)	2.1
Sel Tol (%)	1.0
Sel Xyl (%)	0.1
Sel EtBenz (%)	0.1
Sel C9 Aromatics (%)	0.5
Sel C10 Aromatics (%)	0.7
Sel C9 (%)	0.1
Sel C9= (%)	4.6
Sel C10 (%)	0.4
Sel C10= (%)	0.7
Sel C2-C10 (%)	6.7
Sel C2-C10= (%)	57.4
Sel Aromatics (%)	4.7
Sel C2-C4 (%)	5.1
Sel C2-C4= (%)	28.3

Table S5. Reproducibility of the Fe_2O_3@KO_2/MOR and Fe_2O_3@KO_2/ZSM-5 bifunctional systems at 375 °C, 30 bar, H_2/ CO_2=3, and 5000 $mL \cdot g^{-1} \cdot h^{-1}$.

Sample	**Run**	**Conv. (%)**	**Sel CO (%)**	**Sel C1 (%)**	**Sel C2-C4= (%)**	**Sel Arom. (%)**
Fe_2O_3@KO_2/MOR	1	47.2	12.8	13.3	33.5	2.5
Fe_2O_3@KO_2/MOR	2	48.5	11.9	14.6	32.5	2.7
Fe_2O_3@KO_2/MOR	3	47.9	13.5	13.9	34.4	2.3
Fe_2O_3@KO_2/MOR	4	45.5	13.4	12.5	33.3	3.1
Fe_2O_3@KO_2/MOR	5	46.4	12.9	14.3	32.4	2.1
Fe_2O_3@KO_2/MOR	*Average*	*47.1*	*12.9*	*13.7*	*33.2*	*2.5*
Fe_2O_3@KO_2/ZSM-5	1	48.5	13.9	15.6	12.2	24.1
Fe_2O_3@KO_2/ZSM-5	2	45.1	12.5	13.3	11.1	22.1
Fe_2O_3@KO_2/ZSM-5	3	47.8	14.2	14.8	10.8	23.7
Fe_2O_3@KO_2/ZSM-5	4	48.4	13.9	15.6	13.2	23.3
Fe_2O_3@KO_2/ZSM-5	5	47.3	14.0	15.1	11.6	24.0
Fe_2O_3@KO_2/ZSM-5	*Average*	*47.4*	*13.7*	*14.9*	*11.8*	*23.4*

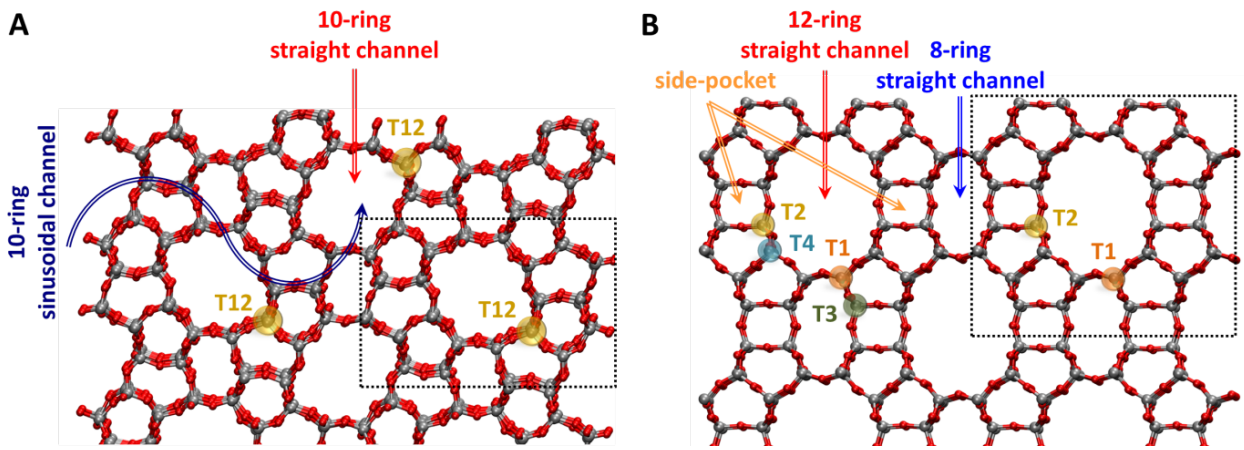

Figure S1. Straight channel view of the of ZSM-5 and MOR zeolite framework with indication of the possible acid sites. The unit cell size is marked by the dotted line.

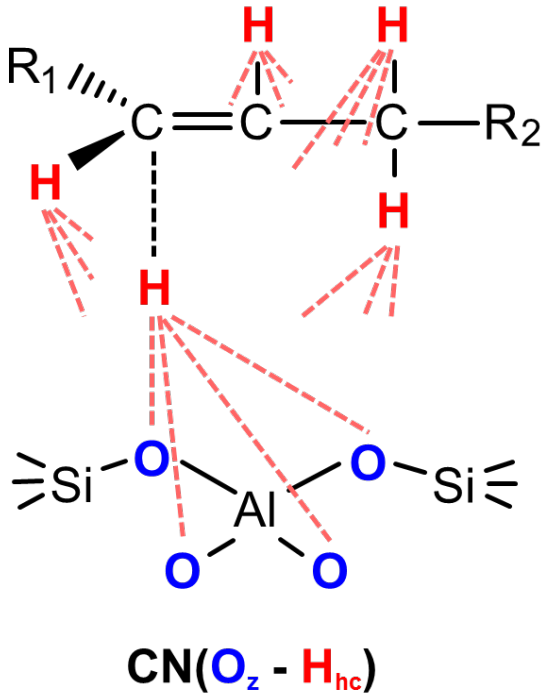

Figure S2. Collective variable (CV) used in the 1D umbrella sampling for alkene protonation.

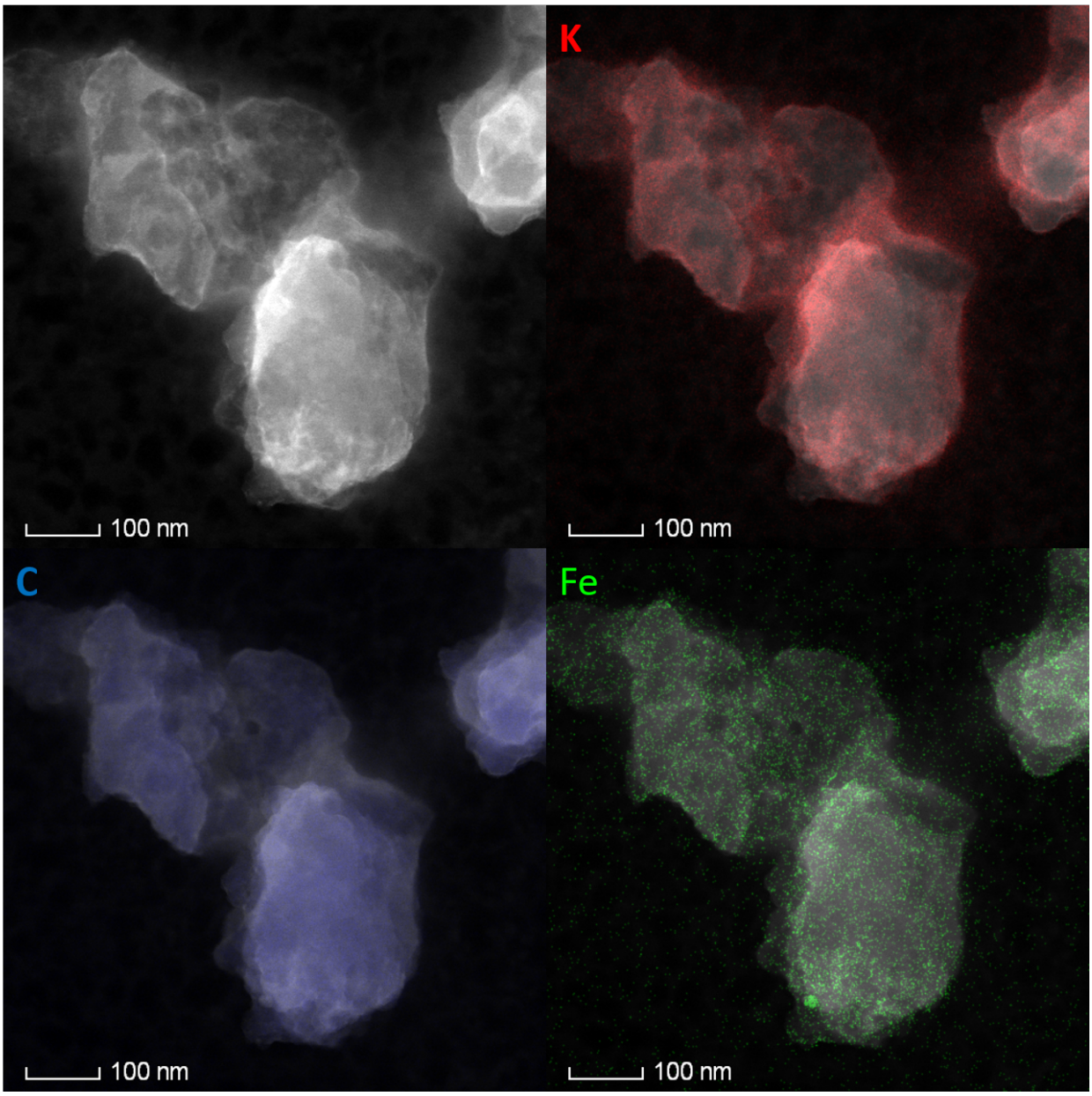

Figure S3. HAADF-STEM of the carbonaceous matrix in the spent Fe_2O_3@KO_2 catalyst.

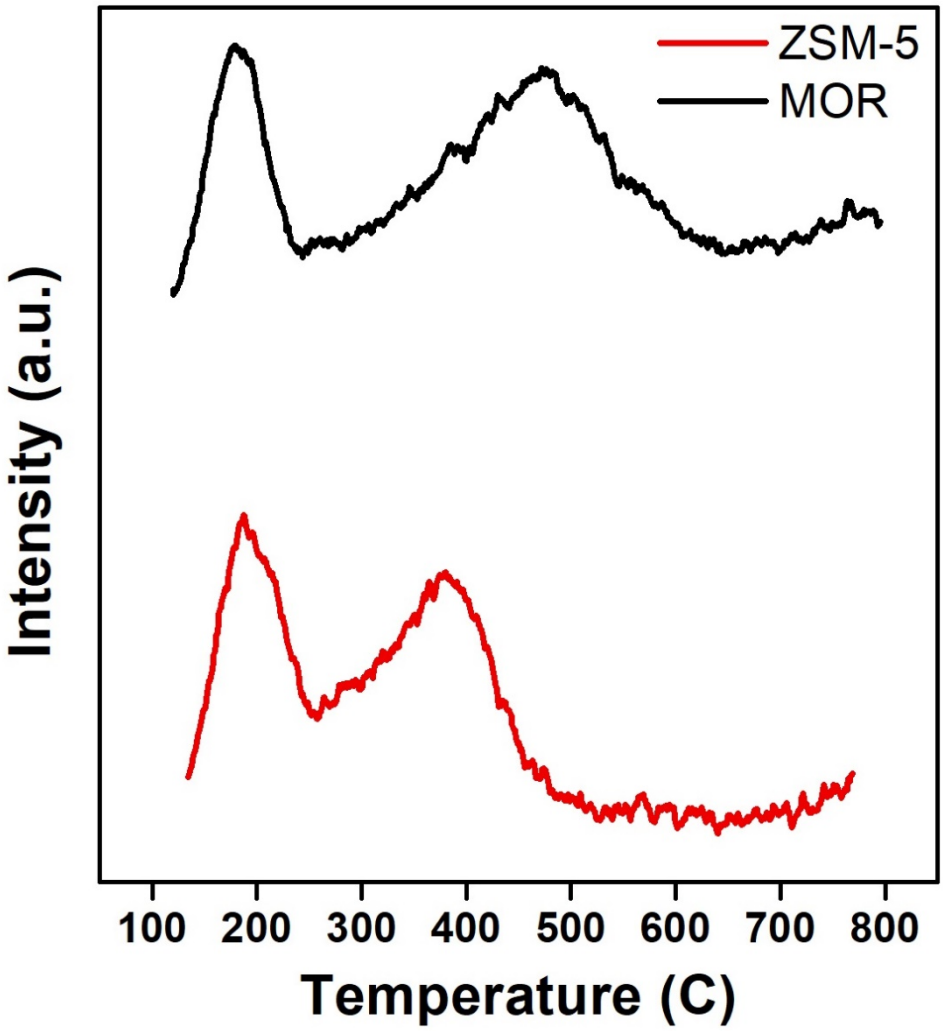

Figure S4. Ammonia temperature programed desorption (TPD) profiles of the ZSM-5 and MOR zeolites.

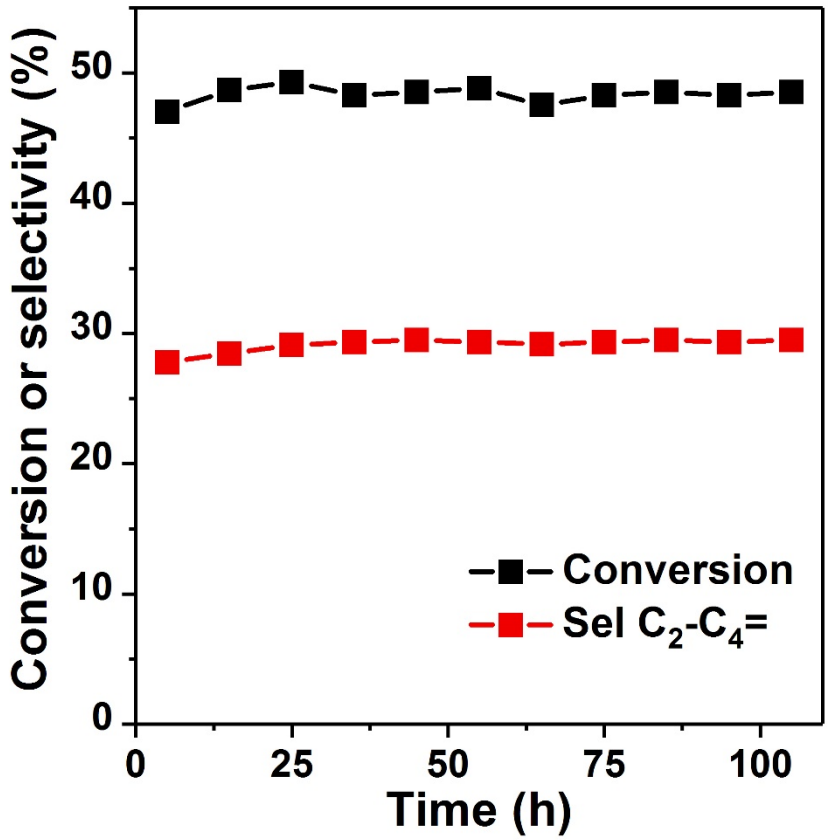

Figure S5. Stability of the Fe_2O_3@KO_2 catalyst during 100h TOS. Reaction conditions: 375 °C, 30 bar, H_2/ CO_2=3, and 10000 $mL \cdot g^{-1} \cdot h^{-1}$.

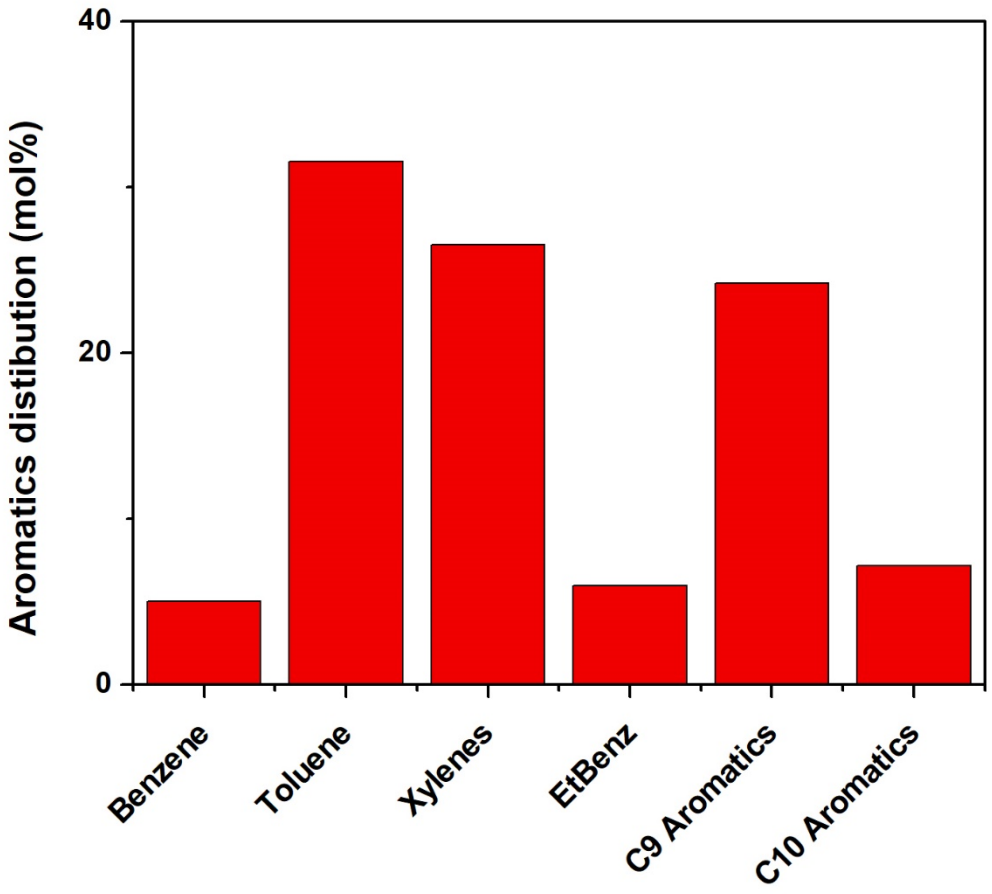

Figure S6. Aromatic distribution of the Fe_2O_3@KO_2/ZSM-5 bifunctional catalyst. 375 °C, 30 bar, H_2/ CO_2=3, and 5000 $mL \cdot g^{-1} \cdot h^{-1}$.

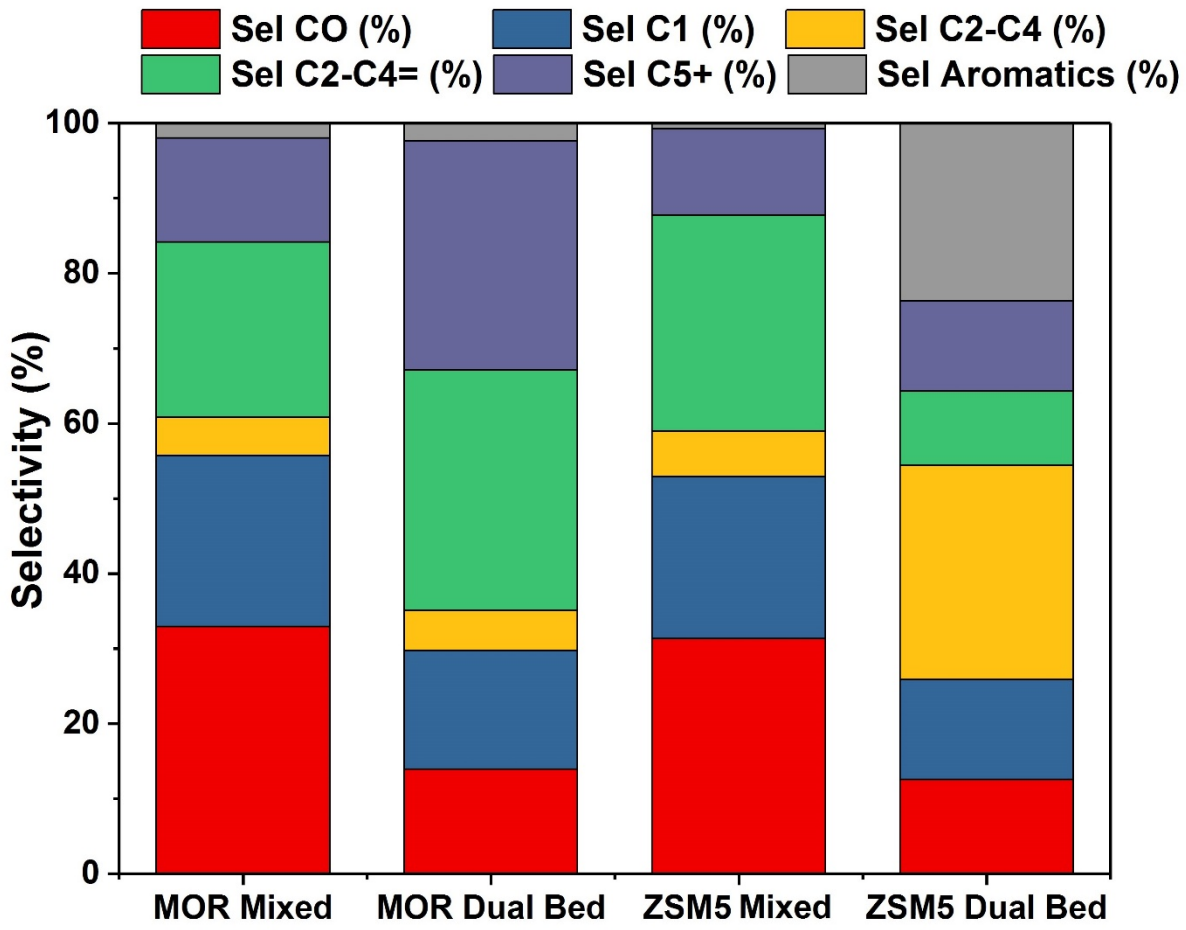

Figure S7. Effect of the spatial arrangement on the product distribution for the Fe_2O_3@KO_2/ZSM-5 and Fe_2O_3@KO_2/MOR bifunctional catalysts. Reaction conditions: 375 °C, 30 bar, H_2/ CO_2=3, and 5000 $mL \cdot g^{-1} \cdot h^{-1}$.

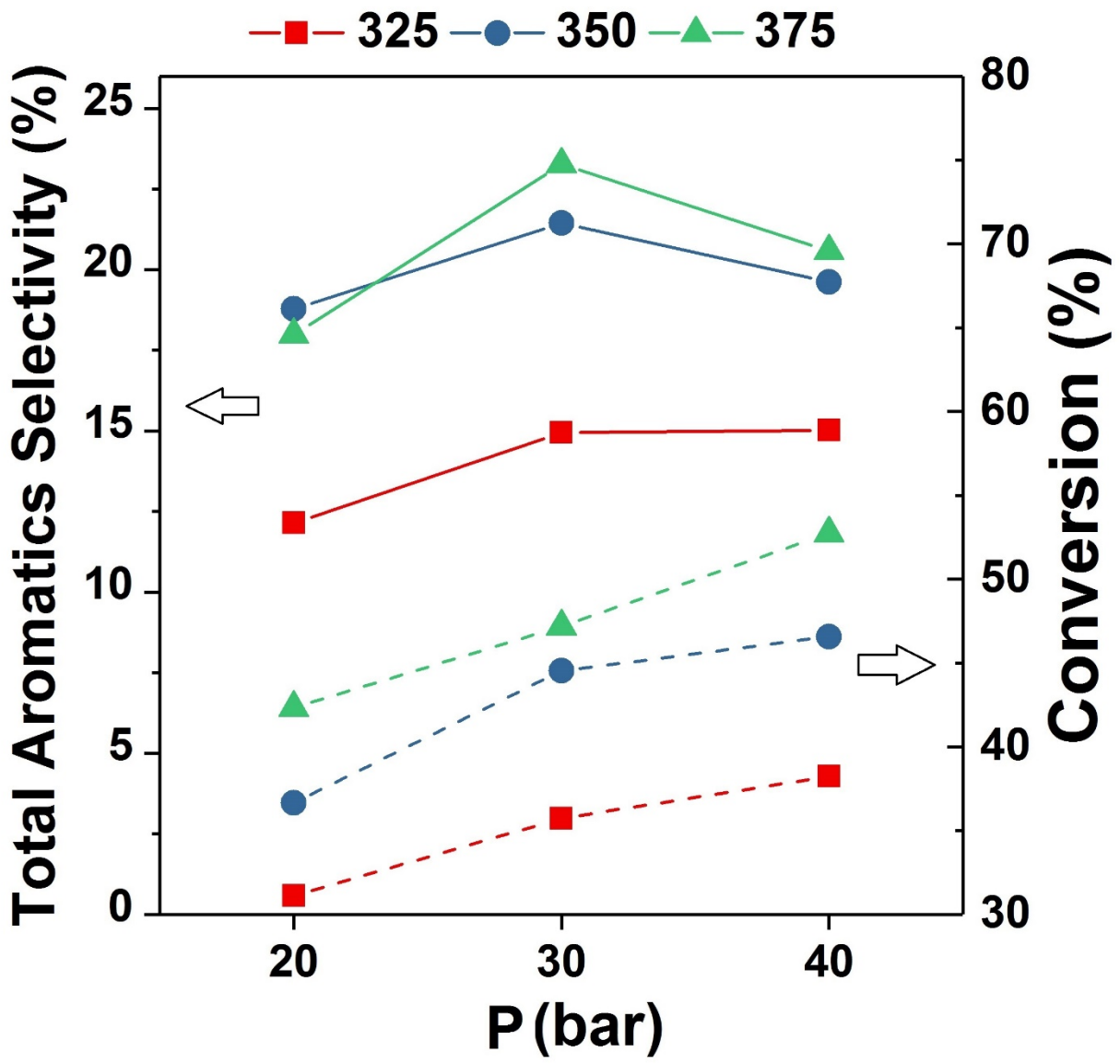

Figure S8. Effect of the reaction conditions on the aromatics selectivity and CO_2 conversion for the Fe_2O_3@KO_2/ZSM-5 bifunctional catalyst.

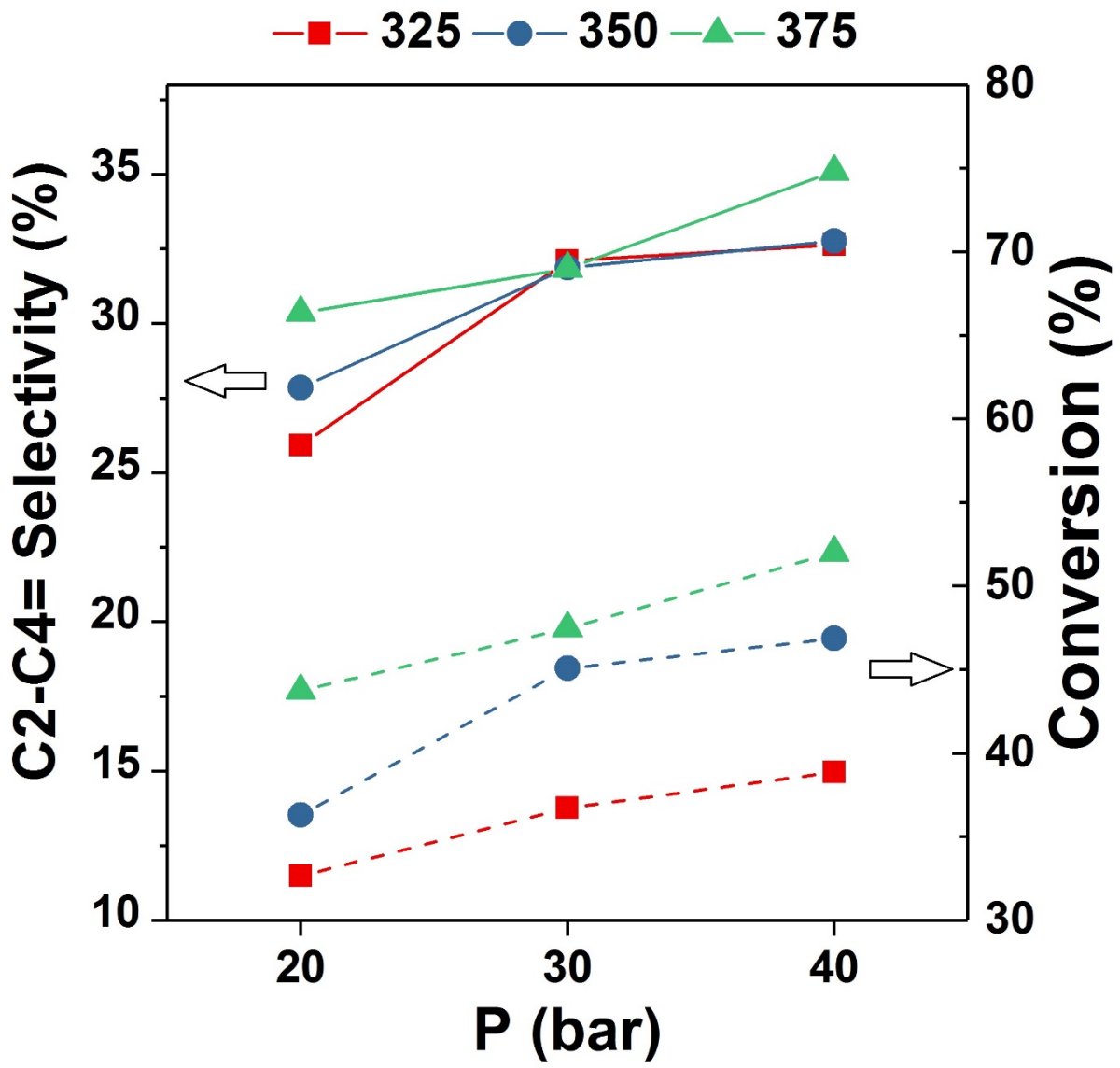

Figure S9. Effect of the reaction conditions on the light olefins selectivity and CO_2 conversion for the Fe_2O_3@KO_2/MOR bifunctional catalyst.

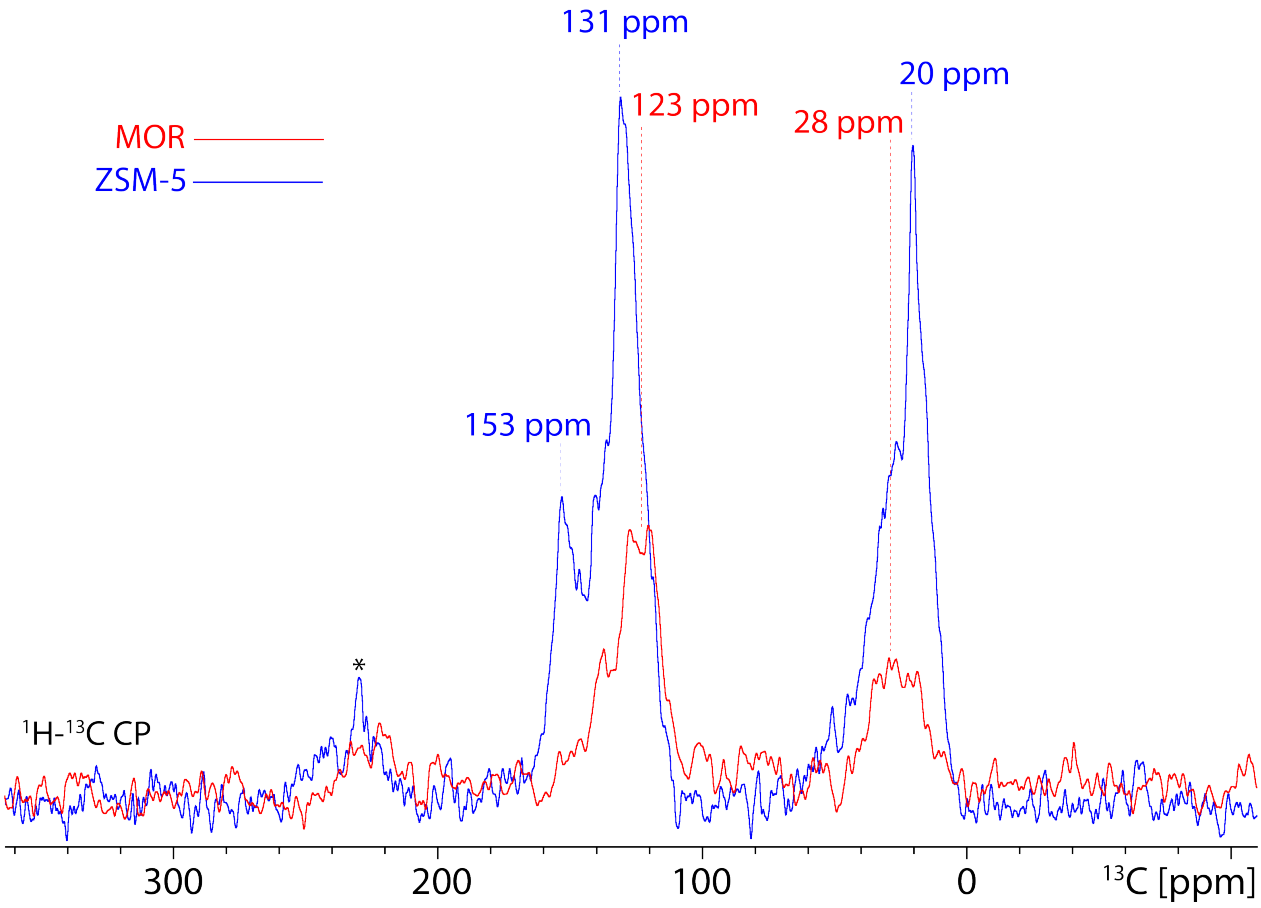

Figure S10. 1D ^{1}H-^{13}C cross-polarization MAS solid-state NMR spectra of zeolite trapped products, i.e. ZSM-5 (blue, 10 kHz MAS, NS=21392) and MOR (red, 10 kHz, NS=36592). The spectra of trapped products are obtained on the post-reacted zeolites after the hydrogenation of carbon dioxide over Fe_2O_3@KO_2/zeolite for 50 hours (* = spinning sideband, NS= number of scans, MAS= magic angle spinning).

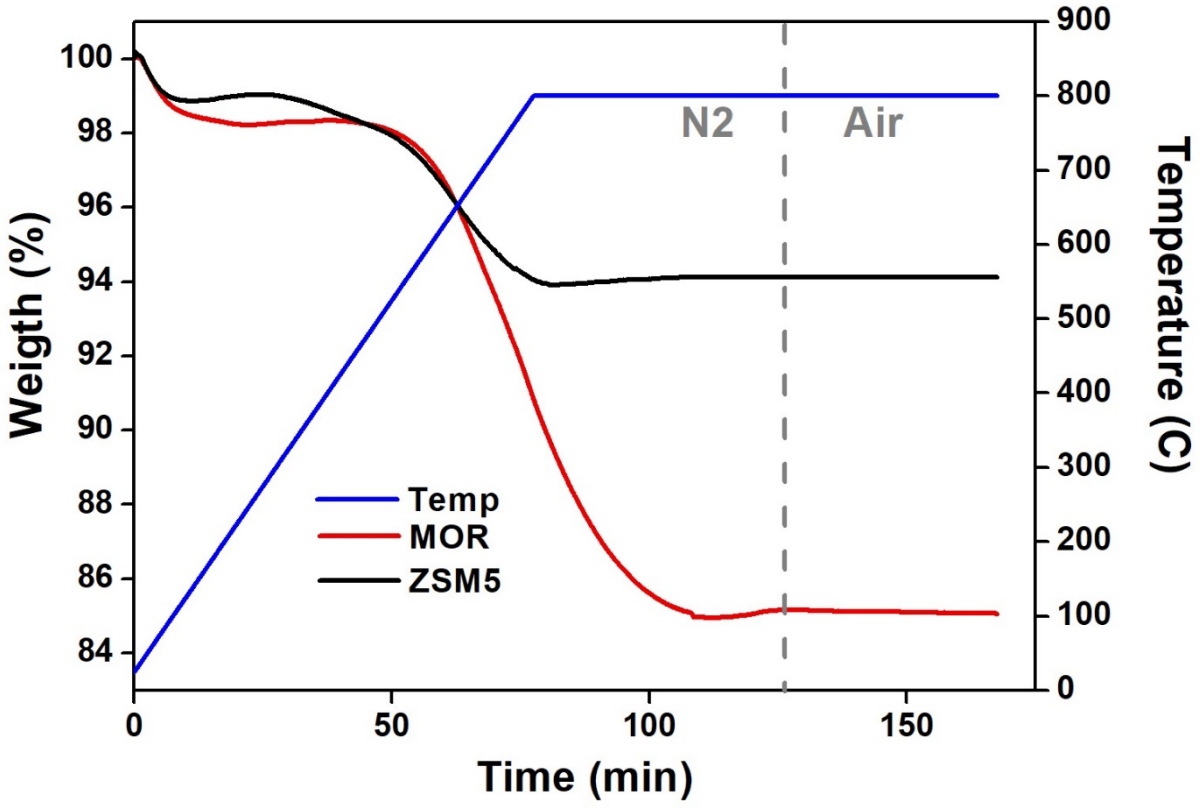

Figure S11. Thermo-gravimetric analysis (TGA) of the spent ZSM-5 and MOR zeolites after 50 hours of reaction.

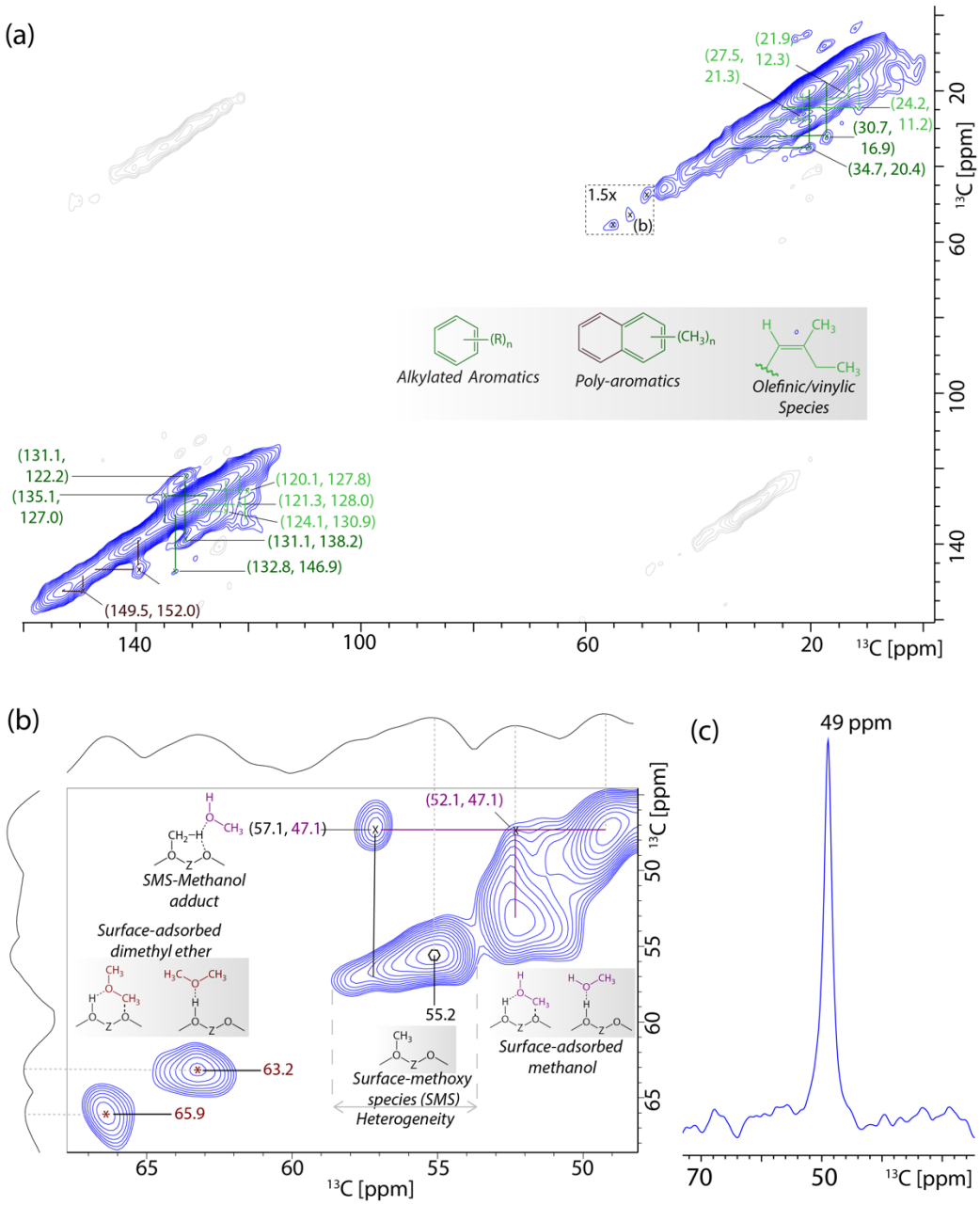

Figure S12. 2D MAS ^{13}C-^{13}C solid-state NMR correlations of identified zeolite ZSM-5 trapped molecular scaffolds: (a) olefinic/vinylic (in light green), mono-aromatics (in green), poly-aromatics (in brown), and (b) alkoxy species (in purple). Spectra obtained on (a) the post-reacted ZSM-5 after the hydrogenation of carbon dioxide over Fe_2O_3@KO_2/ZSM-5 for 50 hours (number of scans = 2048, MAS= magic angle spinning). This measurement also demonstrates the degree of alkylation, such as ethyl groups (for example, 34.7 ↔ 20.4) were identified too along with

methyl groups (see also Figure S11). (b) Zooms of only alkoxy region showcase the existence of surface-adsorbed methanol, surface-methoxy species (SMS), and surface-adsorbed dimethyl ethers in a relatively lower quantity. (C) 1D ^{1}H-^{13}C cross-polarization MAS solid-state NMR spectra of zeolite-adsorbed methanol species. This measurement was performed to confirm the assignment of zeolite surface-adsorbed methanol.

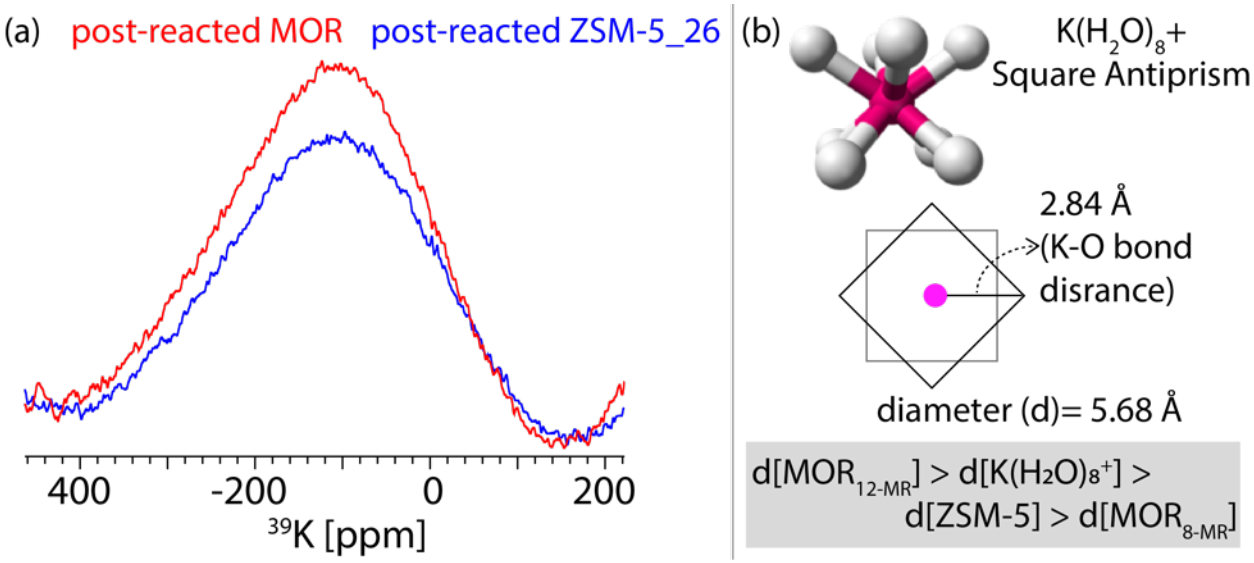

Figure S13. ^{39}K solid-state NMR spectra at 21.1 T and 298 K of (a) post-reacted ZSM-5 (blue, 10 kHz MAS, NS= 60064) and MOR (red, 10 kHz MAS, NS=78208) samples. The very broad spectral feature of both samples possibly could be attributed to the hydrated nature of potassium, i.e. (b) $K(H_2O)_8^+$ (with square antiprism structure), which has been migrated from the metallic part to the zeolitic part of the dual-bed catalytic system during the reaction.

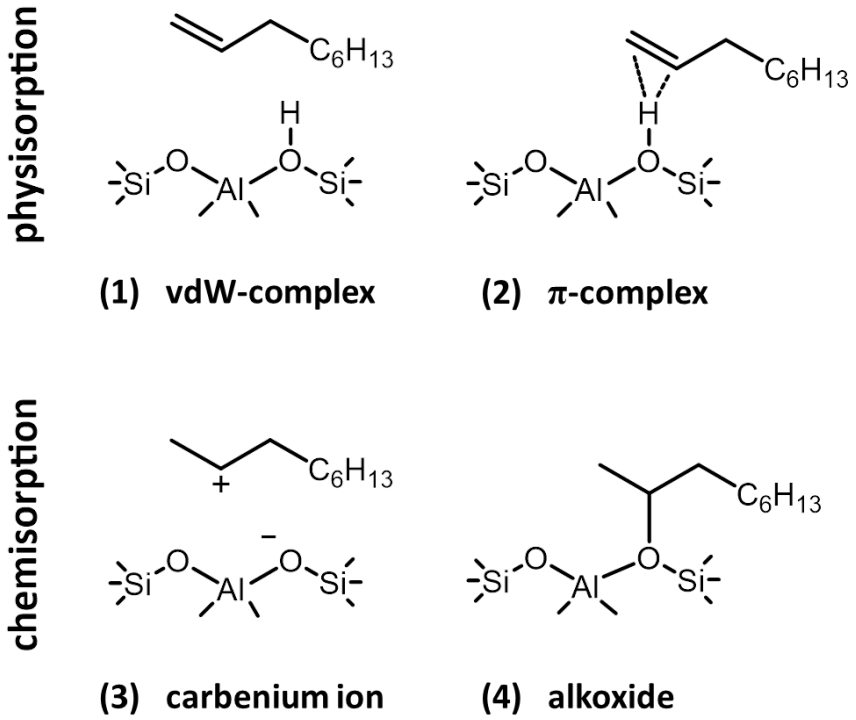

Figure S14. Four adsorption states of 1-nonene – (i) van der Waals complex; (ii) π-complex; (iii) carbenium ion; (iv) alkoxide.

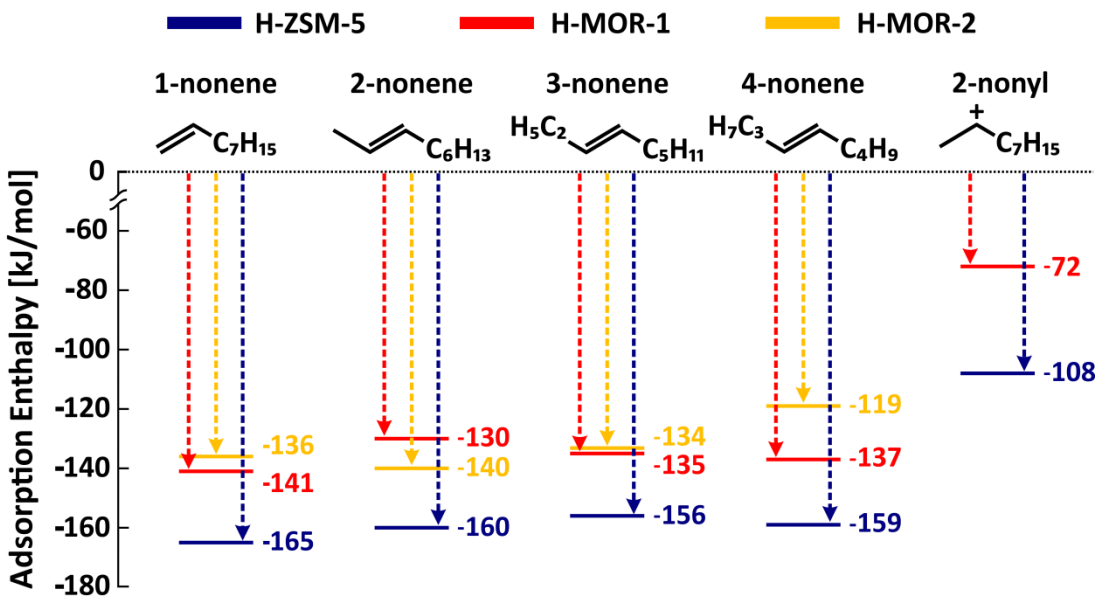

Figure S15. Adsorption enthalpy at 350°C for 1-, 2-, 3-, 4-nonene and 2-nonyl carbenium ion in H-ZSM-5, H-MOR-1 and H-MOR-2 with the empty framework and the respective n-nonene in gas phase as reference state. For the carbenium ion, gas phase 1-nonene and the empty framework are chosen as reference. (Level of theory: PBE-D3)

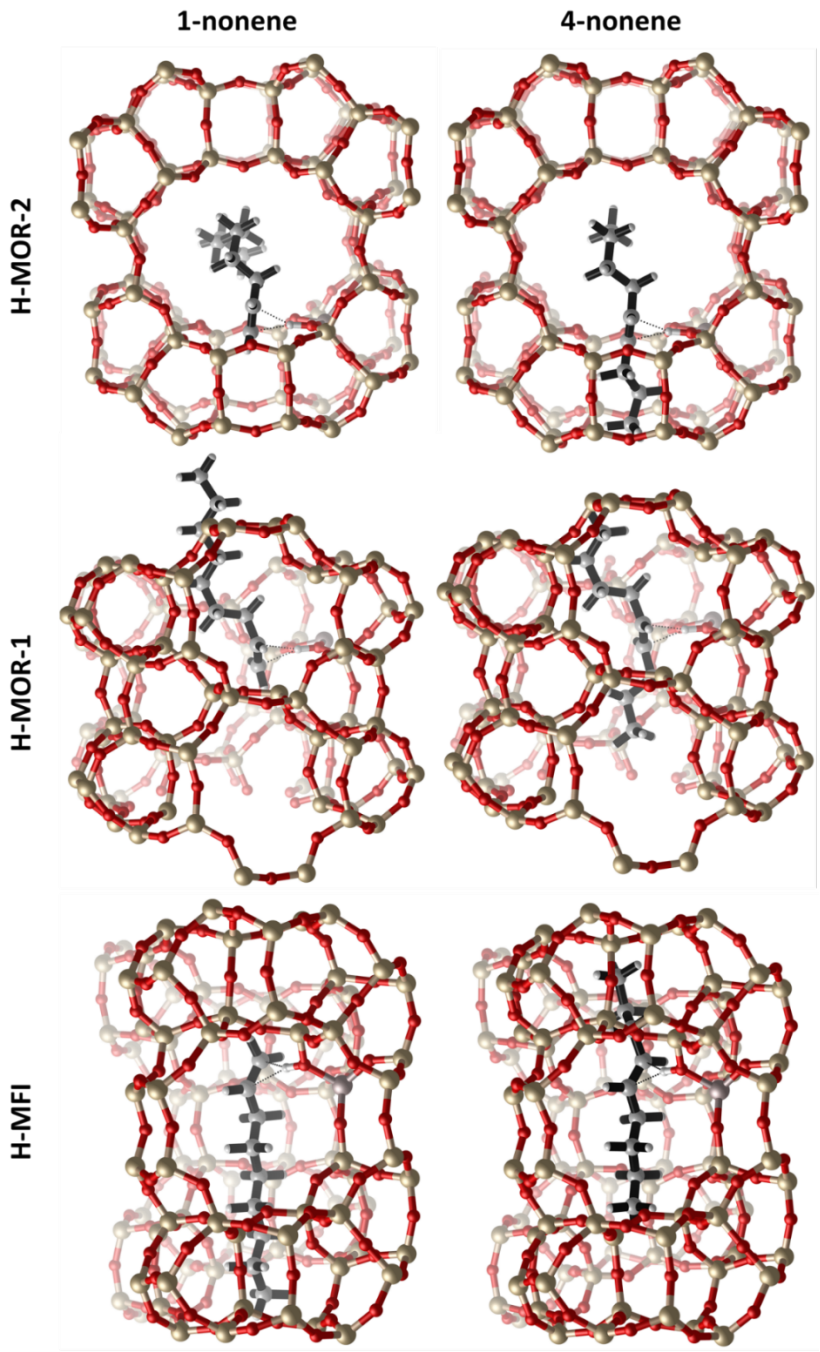

Figure S16. Static geometries of adsorbed 1-nonene (top) and 4-nonene (bottom) π-complez in left: H-MFI (sinusoidal channel view), middle: H-MOR-1 (side pocket view) and right: H-MOR-2 (main channel view).

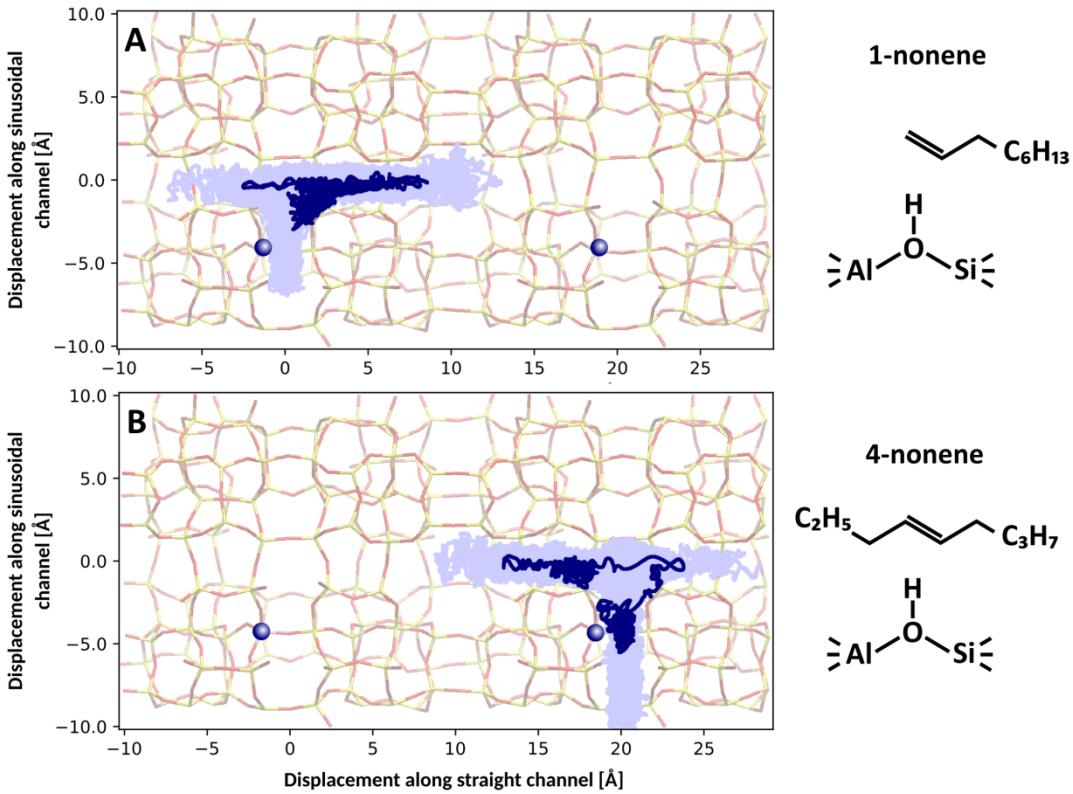

Figure S17. Scatter plot of the mobility of (A) 1-nonene and (B) 4-nonene in the channel system of H-ZSM-5 during the 100 ps MD simulation at 350°C. The acid site is represented by the blue sphere. The occupied unit cell volume is indicated by the light blue color, while the center-of-mass position is plotted in the dark blue color.

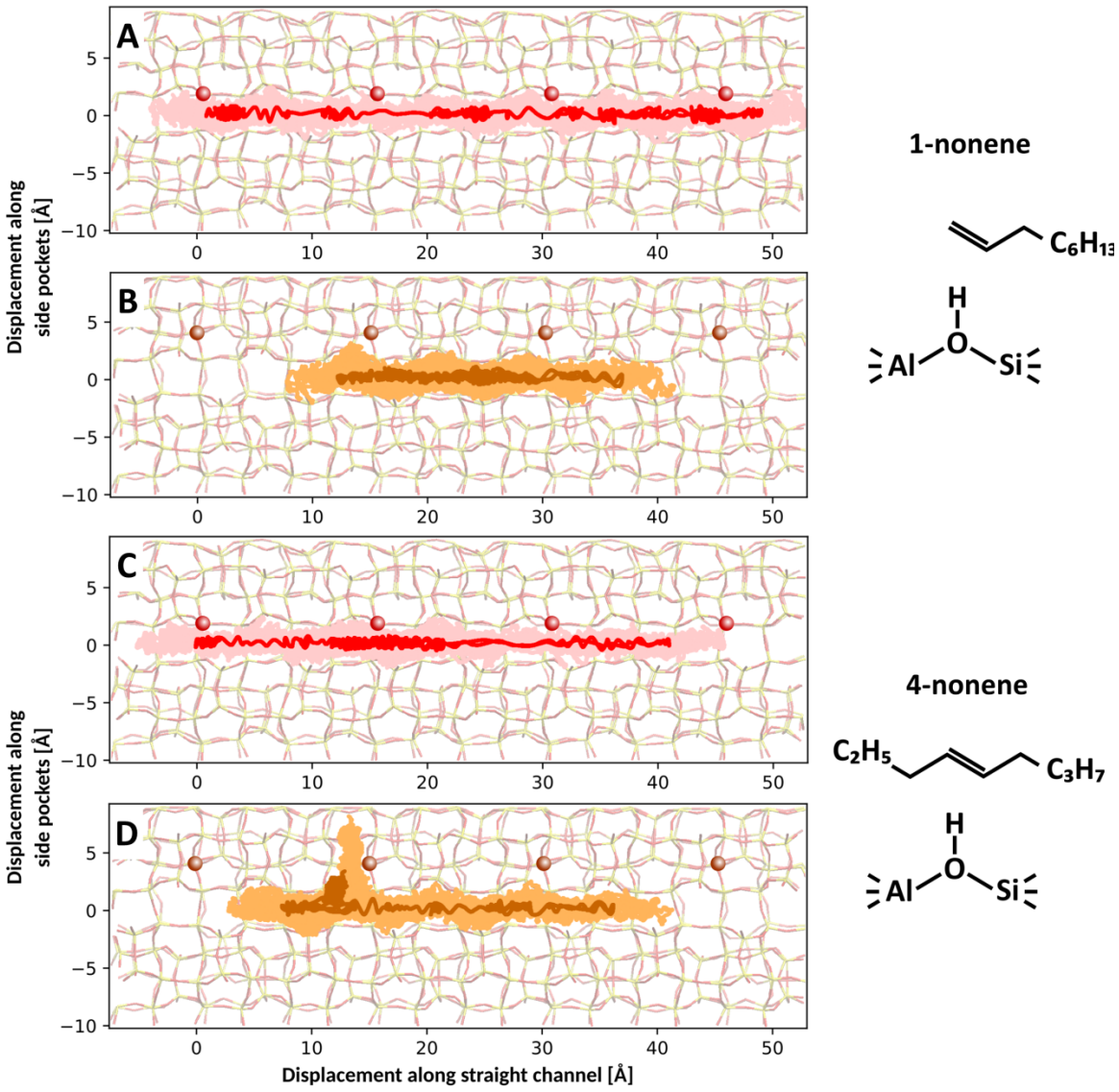

Figure S18. Scatter plot of the mobility of (A) 1-nonene in H-MOR-1, (B) 1-nonene in H-MOR-2, (C) 4-nonene in H-MOR-1 and (D) 4-nonene in H-MOR-2 in the channel system of MOR during the 100 ps MD simulation at 350°C. The acid site is represented by the red (H-MOR-1) or orange (H-MOR-2) sphere. The occupied unit cell volume is indicated by the light color, while the center-of-mass position is plotted in the dark color.

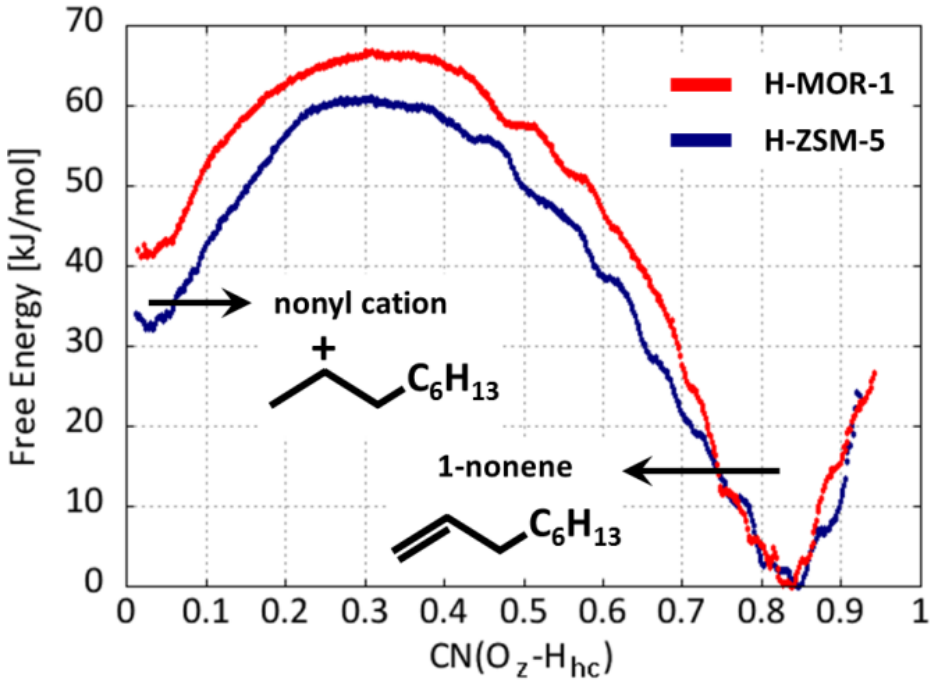

Figure S19. Free energy profiles for the protonation of 1-nonene into a nonyl carbenium ion in H-ZSM-5 (blue) and H-MOR-1 (red) at 350°C. (Level of Theory: revPBE-D3/TZVP-GTH)

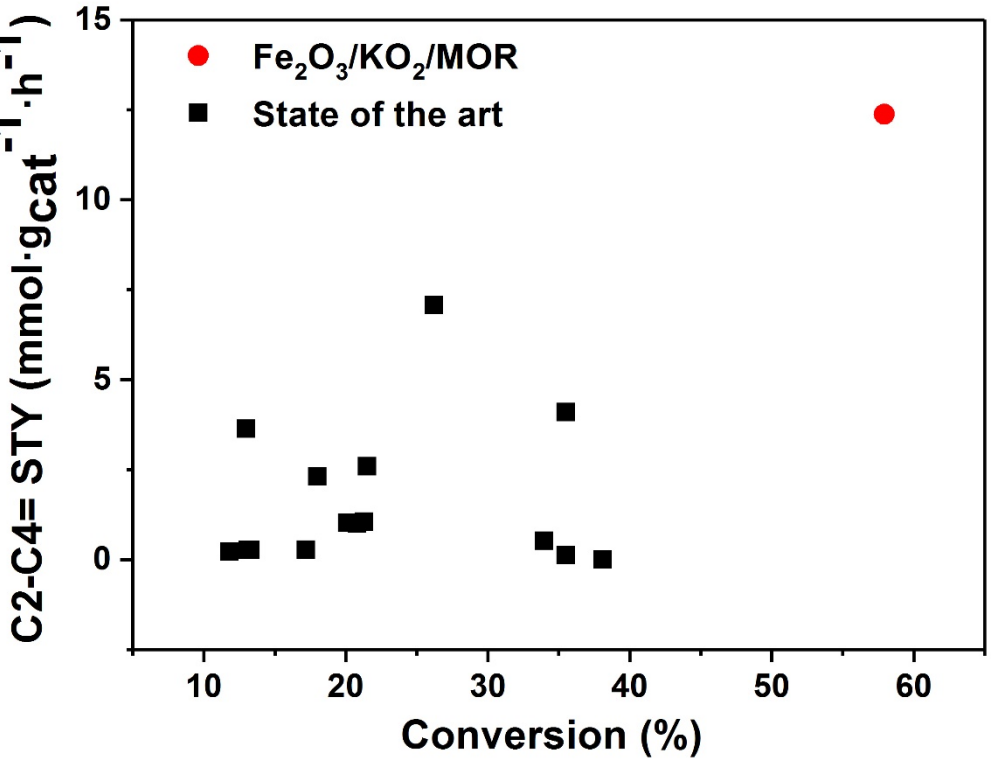

Figure S20. C_2–$C_{4=}$ light olefins STY ($mmol \cdot gcat^{-1} \cdot h^{-1}$) obtained in this work for the Fe_2O_3@KO_2/MOR catalyst compared to the best bifunctional catalysts available for CO_2 hydrogenation.

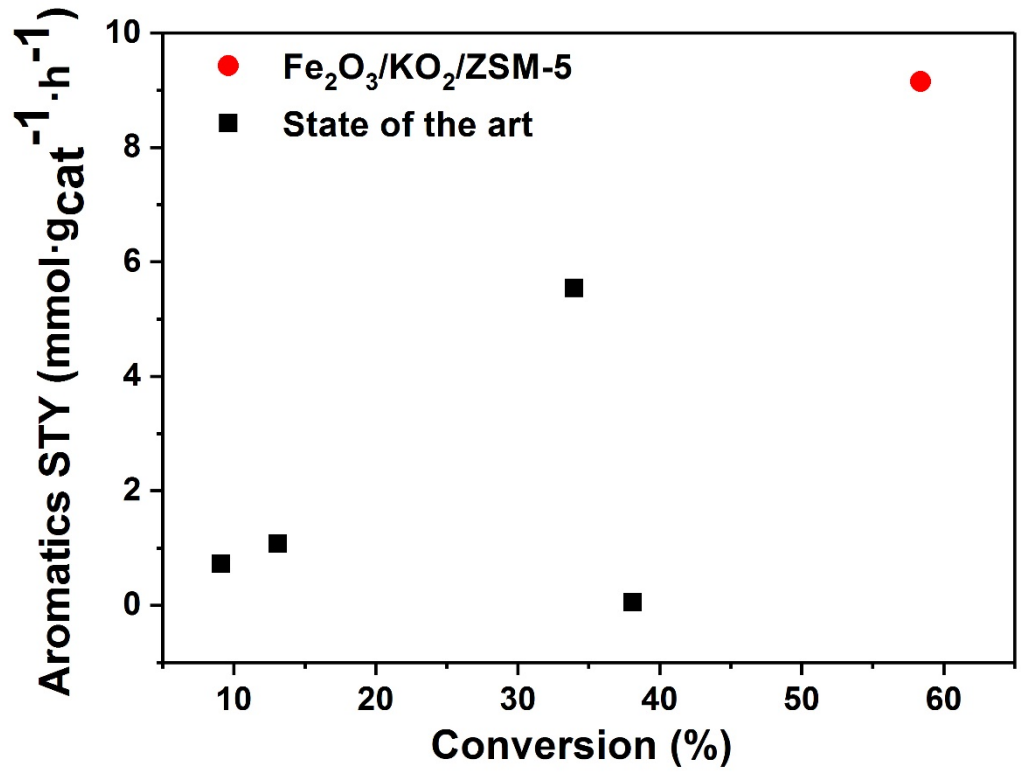

Figure S21. Aromatics STY (mmol·gcat^{-1}·h^{-1}) obtained in this work for the Fe_2O_3@KO_2/ZSM-5 catalyst compared to the best bifunctional catalysts available for CO_2 hydrogenation.